Chemical Science

ROYAL SOCIETY OF CHEMISTRY

EDGE ARTICLE

View Article Online
View Journal | View Issue

Cite this: *Chem. Sci.*, 2020, **11**, 1017

All publication charges for this article have been paid for by the Royal Society of Chemistry

Received 22nd June 2019
Accepted 1st December 2019

DOI: 10.1039/c9sc03095f

rsc.li/chemical-science

How bulky ligands control the chemoselectivity of Pd-catalyzed *N*-arylation of ammonia†

Seoung-Tae Kim, [ab] Suyeon Kim [ab] and Mu-Hyun Baik [*ba]

Steric bulk has been recognized as a central design principle for supporting ligands in the widely utilized Buchwald–Hartwig amination. In a recent example, it was shown that a Pd-catalyst carrying a phosphine ligand can successfully aminate aryl halides using ammonia as the nitrogen source. Interestingly, the chemoselectivity of this reaction was found to depend on the steric demand of the phosphine ligand. Whereas a sterically less demanding phosphine affords diphenylamine as the major product, it was shown that the amination reaction can be stopped after the first amination to give aniline if a sterically more encumbering phosphine ligand is used. Density functional theory calculations were carried out to examine the relationship between the steric demand of the phosphine ligand and the chemoselectivity. It was found that the key feature that leads to the chemoselectivity is the ability of the phosphine ligand to rotate the biaryl moiety of the ligand away from the Pd-center upon amine addition to release some of the steric crowding from the Pd-coordination site.

Introduction

The catalytic formation of C–N bonds is a tremendously important reaction in chemistry and the Pd-catalyzed Buchwald–Hartwig amination is one of the most powerful methods that is used widely in many different applications.[1] Among the substrates that may serve as the nitrogen source of the reaction, ammonia is particularly challenging but interesting. Being the simplest of all amines, it is one of the cheapest and most abundant reactants, making it interesting from practical considerations[2–5] for large scale synthetic applications. From more fundamental perspectives, using ammonia as a reactant poses several challenges. First, ammonia is an excellent ligand and can form very stable Lewis acid–base adducts with transition metals, which often leads to catalyst deactivation. For ammonia to act as an amine source, one of the N–H bonds must be cleaved during catalytic turnover. The N–H bond energy is ~107 kcal mol^{-1} and special provisions must be made to meet this energy demand without making the reaction irreversible. Deprotonation is an obvious strategic alternative to the homolytic N–H bond cleavage, but with the pK_a being ~33, it is not clear at the onset whether this mechanistic pathway offers a decisive advantage.[6–8] If the correct conditions were to be found for an efficient reaction that will form a primary arylamine, for instance, it may become difficult to maintain chemoselectivity, as the primary arylamine product should in principle be a better reactant than ammonia. Thus, mixtures of primary and secondary amines are anticipated and engineering chemoselectivity in these reactions becomes a necessary challenge that must be overcome to design a useful synthetic method. Several successful methods for the selective arylation of ammonia using transition metal catalysts have been reported recently.[9–14] Buchwald reported an intriguing Pd-catalyzed example using a biaryl phosphine ligand. Interestingly, the chemoselectivity towards the primary or secondary arylamine product was shown to be controlled by the steric demand of the phosphine ligand, as summarized in Scheme 1.[15,16] Whereas the sterically less demanding **L1** ligand gave only the secondary amine, the chemoselectivity could be completely switched to the primary amine product even at aryl halide concentrations above 0.05 M [16] by decorating one of the biaryl moieties with Me and OMe functionalities as shown for **L3** and **L4** in Scheme 1. While the increased conformational rigidity resulting from the 3- and 6-methyl (or methoxy) groups in the biaryl backbone (**L2**, **L3** and **L4**) was suggested to be a key component for the selectivity inversion,[15] the precise mechanism of how the substitution switches the selectivity was unclear. Intuitively, increasing the steric demand of the phosphine ligand to disfavour the binding of the primary amine *vs.* ammonia is plausible. To obtain a more precise understanding of the features that control the chemoselectivity, we employed quantum chemical molecular modelling methods based on density functional theory (DFT) to construct a full catalytic cycle of the Pd-catalyzed chemoselective arylation reaction.

[a]*Department of Chemistry, Korea Advanced Institute of Science and Technology (KAIST), Daejeon 34141, Republic of Korea. E-mail: mbaik2805@kaist.ac.kr*

[b]*Center for Catalytic Hydrocarbon Functionalizations, Institute for Basic Science (IBS), Daejeon 34141, Republic of Korea*

† Electronic supplementary information (ESI) available: Cartesian coordinates and energies of all computed structures are provided. See DOI: 10.1039/c9sc03095f

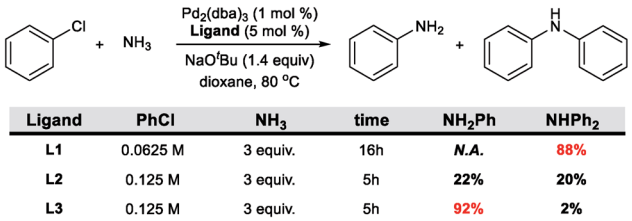

Ligand	PhCl	NH_3	time	NH_2Ph	$NHPh_2$
L1	0.0625 M	3 equiv.	16h	*N.A.*	88%
L2	0.125 M	3 equiv.	5h	22%	20%
L3	0.125 M	3 equiv.	5h	92%	2%
L4	0.125 M	3 equiv.	5h	89%	4%

Ligand =

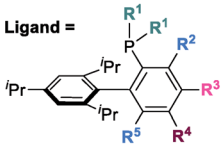

L1 : R^1 = Cy, $R^{2,3,4,5}$ = H
L2[a] : R^1 = ^{i}Pr, $R^{2,4,5}$ = Me, R^3 = OMe
L3[a] : R^1 = Cy, $R^{2,4,5}$ = Me, R^3 = OMe
L4 : R^1 = ^{t}Bu, $R^{2,5}$ = OMe, $R^{3,4}$ = H

[a] A mixture of two isomers was used for the experiment.

Scheme 1 Previous experimental results of *N*-arylation with four different ligands. The bulkiness of a ligand increases from L1 to L4.

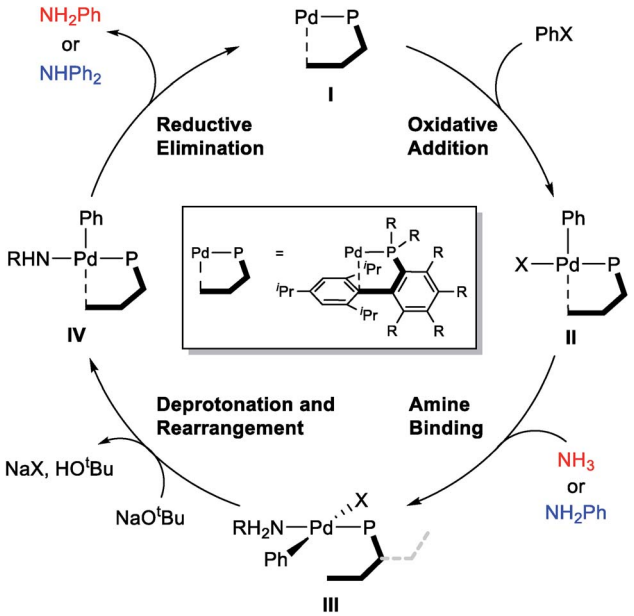

Scheme 2 The general mechanism of the Pd-catalyzed *N*-arylation reaction.

Experimental

Computational details

All density functional theory (DFT) calculations were performed using the Jaguar 9.1 quantum chemistry program.[17] Electronic exchange and correlation energy contribution to the total electronic energy was approximated with the B3LYP hybrid functional[18,19] along with Grimme's D3 [20] dispersion correction (B3LYP-D3). All intermediate and transition state geometries were optimized with the 6-31G** basis set[21–23] for main group atoms. Pd was described by the Los Alamos relativistic effective core potential (ECP)[24–26] and its corresponding LACVP basis set. While these basis sets are adequate for obtaining geometries, more reliable energies were obtained from the single point calculations using Dunning's correlation-consistent triple-ζ basis set, cc-pVTZ(-f),[27] for main group and larger LACV3P for Pd. The zero-point energy (ZPE), entropic and solvation contributions to the Gibbs energy are obtained at the same level of theory as the geometry optimizations (B3LYP-D3/6-31G**/LACVP). The optimized geometries characterized as the local minima on the potential energy surfaces do not contain any imaginary frequency, while each of the transition states contains one imaginary frequency. The solvation calculations utilized the self-consistent reaction field (SCRF) approach using a standard Poisson–Boltzmann solver[28–30] on the gas phase geometry to model the solvation shell of dielectric constant $\varepsilon = 2.209$, which we consider to be an approximate solvation environment offered by the 1,4-dioxane.

Results and discussion

The general mechanism of the Pd-catalyzed Buchwald–Hartwig C–N cross-coupling reaction is well established,[31–46] and the main features are summarized in Scheme 2. The catalytic cycle starts with the oxidative addition of the aryl halide substrate to afford intermediate **II**, which can bind the amine substrate to give a square-planar, 16-electron Pd(II)-intermediate **III**. The key deprotonation event takes place next with the assistance of an external base, such as NaO^{t}Bu, accompanied by the loss of the halide ligand to form a formally under-coordinated Pd-complex where the fourth coordination site is occupied by the aryl moiety of the sterically bulky phosphine ligand. Finally, reductive elimination gives the final amination product and reforms the Pd(0) catalyst.

Proximal *vs.* distal conformation

Given the general pattern of the catalytic cycle, there are several steps where the steric bulk of the ligand can impact the reaction. Before these features are examined in detail, it is helpful to first study the impact of the functionalization on the chemical properties of the phosphine ligand itself. Scheme 1 summarizes the previously reported experimental results for four representative ligands that we studied in detail in this work. One key feature of the phosphine ligands carrying a biaryl appendage is their ability to move the sterically demanding biaryl unit into the coordination site of the Pd-center or move it away when needed. Empirically, it is known that the substitution at the C6 position tends to accelerate the reductive elimination step by increasing the steric congestion (Fig. 1),[47] which is easy to understand. It is not clear, however, how the steric congestion may impact the reaction of the primary amine compared to ammonia at this step. In 2007, Buchwald examined how the amine substrate binds to Pd(II),[33,48] and suggested that the increased steric demand due to the amine binding may induce the distal-form of the Pd-complex, where the biaryl moiety is rotated away from the Pd-center, as illustrated in Fig. 1. It is plausible to expect that this rotation will be significantly impacted by the presence of the additional R^2 substituents on the phosphine-containing aryl ring and also be influenced by the bulkiness of the R^1 group on the phosphine. Fig. 1 shows a potential energy surface scan along the Pd–P–C1–C2 dihedral

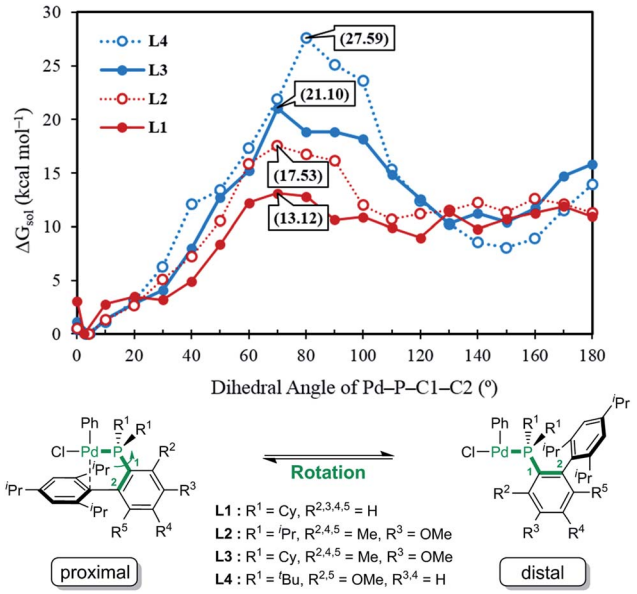

Fig. 1 Relative free energy of the oxidative addition Pd-complex *vs.* varying dihedral angles (Pd–P–C1–C2) depending on the ligand, **L1**, **L2**, **L3** and **L4**.

angle, where 19 structures were optimized with a constrained Pd–P–C1–C2 dihedral angle ranging from 0° to 180°. Reaching a geometry that would give the distal-form of **L1** is found to be uphill in energy, with the highest energy conformers being in the range of 13 kcal mol^{-1}. Note that the actual rotation barrier is likely to be a few kcal mol^{-1} higher than what was found for the highest energy conformer.

As expected, the ligands that acquire further rigidity *via* R^2 and R^5 substitutions demand higher energies to approach the distal-form. Depending on the steric bulkiness of the R^1 (^{i}Pr = **L2**, Cy = **L3**, or ^{t}Bu = **L4**) groups, the substitutions increase the energy of the highest conformer to 18, 21 and 28 kcal mol^{-1}, respectively, as shown in Fig. 1. Notably, the ~3 kcal mol^{-1} higher energy of **L3** over **L2** is the result of the rigidity of Cy in **L3** over ^{i}Pr in **L2** (see ESI† for details). These energy profiles indicate that the transition to the distal geometry becomes highly improbable for **L3** and **L4**, whereas the (**L1**/**L2**)Pd complexes may adopt the distal-form with ease to accommodate amine binding.

Mechanism using L1

Considering the conceptual understanding of how the increased steric demand impedes the rotation of the biaryl functionality, which is key for the switch between the "distal" and "proximal" orientation of the biaryl ligand, the complete reaction mechanism was modelled using the **L1** ligand, as shown in Fig. 2. The reaction energy profile for processing ammonia is shown in red, whereas the reaction using aniline as the substrate is given in blue. As discussed above, oxidative addition of phenyl chloride starts the catalytic cycle and the

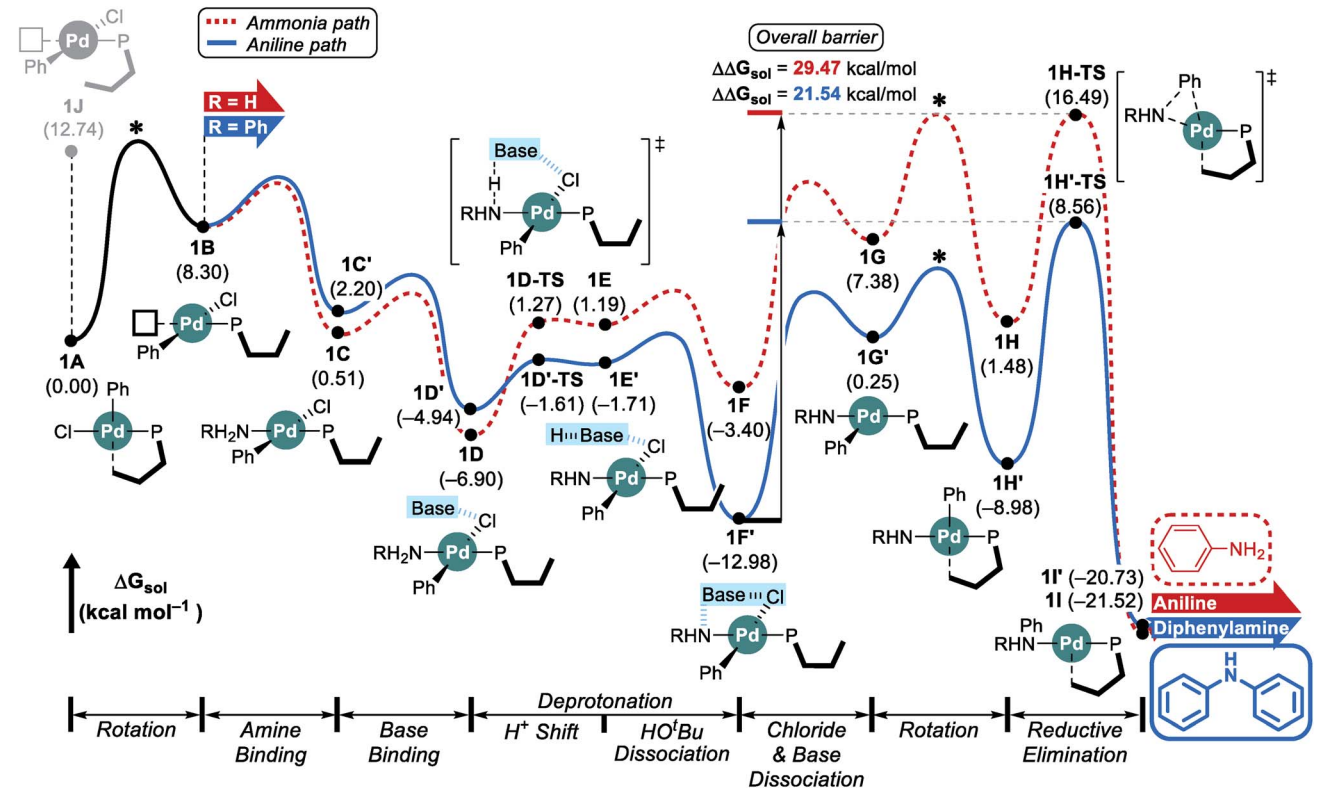

Fig. 2 DFT-calculated energy profile for Pd-catalyzed *N*-arylation with **L1**. * represents the rotation barrier which is estimated to be over 13 kcal mol^{-1}.

barrier associated with the computed transition state is only 10.1 kcal mol^{-1}, which is consistent with rapid oxidative addition to give the first key intermediate **1A**.[47] With a less bulky ligand **L1**, the oxidative addition complex **1A** readily rotates the biaryl ring with an estimated barrier of 13 kcal mol^{-1} and prefers to yield the distal form intermediate **1B** rather than **1J** which keeps the biaryl position fixed while undergoing rearrangement for the subsequent amine coordination. Since the proximal-conformer **1J** located at 12.7 kcal mol^{-1} has an energy that is comparable to the rotation barrier and the distal-conformer **1B** is computed to be 4.4 kcal mol^{-1} more stable than **1J** due to the smaller steric congestion, the reaction will proceed through the distal pathway when **L1** is used.

After the ligand rearrangement, the amine/ammonia binding and subsequent deprotonation assisted by NaO^{t}Bu push the reaction forward. Note that NaO^{t}Bu base is modelled in its tetrameric form considering the non-polar environment of the reaction, as illustrated in Scheme 3.[49–51] The *tert*-butoxide is also examined as an active base but was found to be less probable in this system since this model failed to properly explain the observed chemoselectivity (see ESI† for details).

Since ammonia is the only substrate available at the beginning, the initial reaction follows the pathway shown in red to produce aniline. The binding of ammonia to **1B** yields the intermediate **1C** that has the same ligand arrangement as the reported crystal structure.[33] Next, the NaO^{t}Bu base binds to **1C** to give intermediate **1D** at a free energy of −6.9 kcal mol^{-1}. As discussed above, deprotonation of ammonia is challenging, despite the utility of the strong base NaO^{t}Bu, and the deprotonated intermediate **1E** is ∼8 kcal mol^{-1} higher in energy. Dissociation of *tert*-butanol and extraction of the chloride anion, which becomes incorporated into the NaO^{t}Bu tetramer, ensure charge neutrality of this step and result in the intermediate **1F** at −3.4 kcal mol^{-1}. Release of the base that carries the chloride anion gives the putative intermediate **1G**, which is the 3-coordinate intermediate carrying the aryl and amido groups, in addition to the phosphine ligand. This intermediate is shown in Fig. 2, but is unlikely to exist, as rotation of the biaryl moiety of the phosphine ligand will easily give access to the proximal form to restore the Pd–C$_{ipso}$ interaction and lower the energy of the Pd-complex by ∼6 kcal mol^{-1} in **1H**. The amido-nitrogen can now form a C–N bond in a reductive elimination step. The transition state **1H-TS** is found at 16.5 kcal mol^{-1} resulting in an overall barrier of 23.4 kcal mol^{-1}, $\Delta_r G$(**1D** → **1H-TS**), which is reasonable to be overcome under the given experimental conditions.

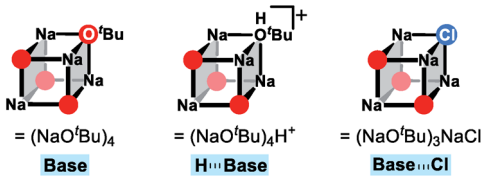

Scheme 3 Schematic illustration of the tetrameric form of NaO^{t}Bu and its derivatives.

As the catalytic reaction proceeds, aniline and ammonia start to compete as reactants. And our calculations indicate that the binding of aniline is energetically less favoured by 1.7 kcal mol^{-1} compared to ammonia, which is in good agreement with the intuitive expectation that ammonia should be a better ligand for Pd(II) than aniline. But as demonstrated in a previous study from the Buchwald group, the amine binding preference does not affect the chemoselectivity,[48] because this step is associated with very low energies and the amine binding is expected to be fully reversible with little impact on the overall selectivity. Our calculations predict that aniline is much easier to deprotonate and the key intermediate **1F′** is found at a relative energy of −13.0, which is nearly 10 kcal mol^{-1} lower than its analogue **1F**, as illustrated in Fig. 2. Intermediate **1F′** is of utmost importance, as it is the lowest energy intermediate of the whole catalytic cycle. With both aniline and ammonia present in solution, the two reaction pathways are connected through the common intermediate **1B**. Thus, intermediate **1F′** formally coexists by establishing an equilibrium with **1F** *via* intermediate **1B**, where the aniline reactant is exchanged with ammonia. Consequently, the rate determining barriers for both ammonia and aniline reactions must be evaluated from intermediate **1F′**. Doing so, our calculations suggest that the overall barrier for reductive elimination using aniline is 21.5 kcal mol^{-1}, $\Delta_r G$(**1F′** → **1H′-TS**), whereas that for ammonia in the presence of aniline becomes 29.5 kcal mol^{-1}, $\Delta_r G$(**1F′** → **1H-TS**), as highlighted in Fig. 2. Therefore, the C–N coupling reaction with **L1** is expected to convert aniline that is initially produced to give the diphenylamine product quantitatively, as shown in blue in Fig. 2.

Scheme 4 summarizes the difference of the two substrates that is described in the energy profile. The distinct feature of aniline originates from the interaction between the lone pair of nitrogen and the π-system of its Ph group that lowers its binding affinity and nucleophilicity. The relatively weak binding affinity of aniline gives rise to a Pd–N bond that is 0.041 Å longer

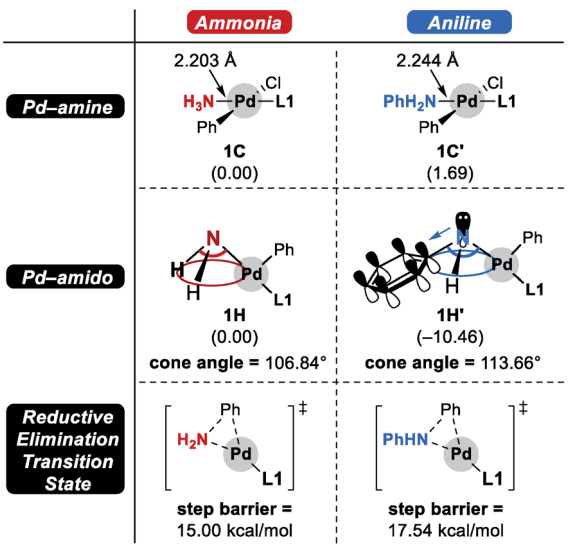

Scheme 4 Comparison of two substrates, ammonia and aniline.

and 1.7 kcal mol^{-1} higher intermediate energy of **1C′** compared to **1C**. Whereas the resonance in aniline involving the lone-pair of nitrogen makes **1C′** less stable, this effect facilitates the generation of an amido group where additional lone-pair electrons are formed through deprotonation of the amine substrate. This effect drives the energy to be 10.5 kcal mol^{-1} lower and the cone angle is wider by 6.82° in **1H′** than in **1H**. The difference of nucleophilicity also impacts the reductive elimination step where the amido moiety acts as a nucleophile to form the C–N bond. Our calculations show that the step barrier for reductive elimination in **1H** is 2.5 kcal mol^{-1} lower than that of **1H′**, in good agreement with intuitive expectations.

Mechanism using L2

The reaction with the **L2** ligand furnishes both aniline and diphenylamine in almost identical amount with 54% conversion over a reaction time of 5 h (Scheme 1),[18] while our calculations predict that this reaction should eventually generate diphenylamine dominantly. When interpreting quantum chemically calculated reaction energy profiles, it is important to recognize that the calculated barriers can only give an estimate for the reaction rate. Because it is not possible to reliably estimate the preexponential frequency factor of the Arrhenius equation, it is not possible to reliably represent the reaction rates. Matching experiments to computational models becomes particularly challenging, if the reaction does not convert completely, as is the case here. These limitations notwithstanding, we can still extract some useful information from our calculations using the **L2** ligand. Although the functionalization at C3 and C6 positions makes the ligand more sterically bulky and escalates the rotation barrier to over 17 kcal mol^{-1}, the increased steric congestion destabilizes the proximal conformer **2I** at the same time and results in a free energy of 17.8 kcal mol^{-1} (Fig. 3). Thus, as was observed using **L1**, the distal pathway will also be slightly preferable with the **L2** ligand. In addition to the rotation barrier increment, the functionalization accelerates the reductive elimination and therefore, the rotation step becomes the most difficult step in the reaction with **L2**. From the ground state intermediate **2E′** which has a relative free energy of −11.7 kcal mol^{-1}, the rotation barrier to access **2G** is presumably higher than 31 kcal mol^{-1}. Consequently, as the reaction proceeds toward completion and the concentration of ammonia diminishes while that of aniline increases, the aniline pathway shown in blue will be preferred and yield diphenylamine dominantly. Overall, our calculation results predict that diphenylamine should be the major product

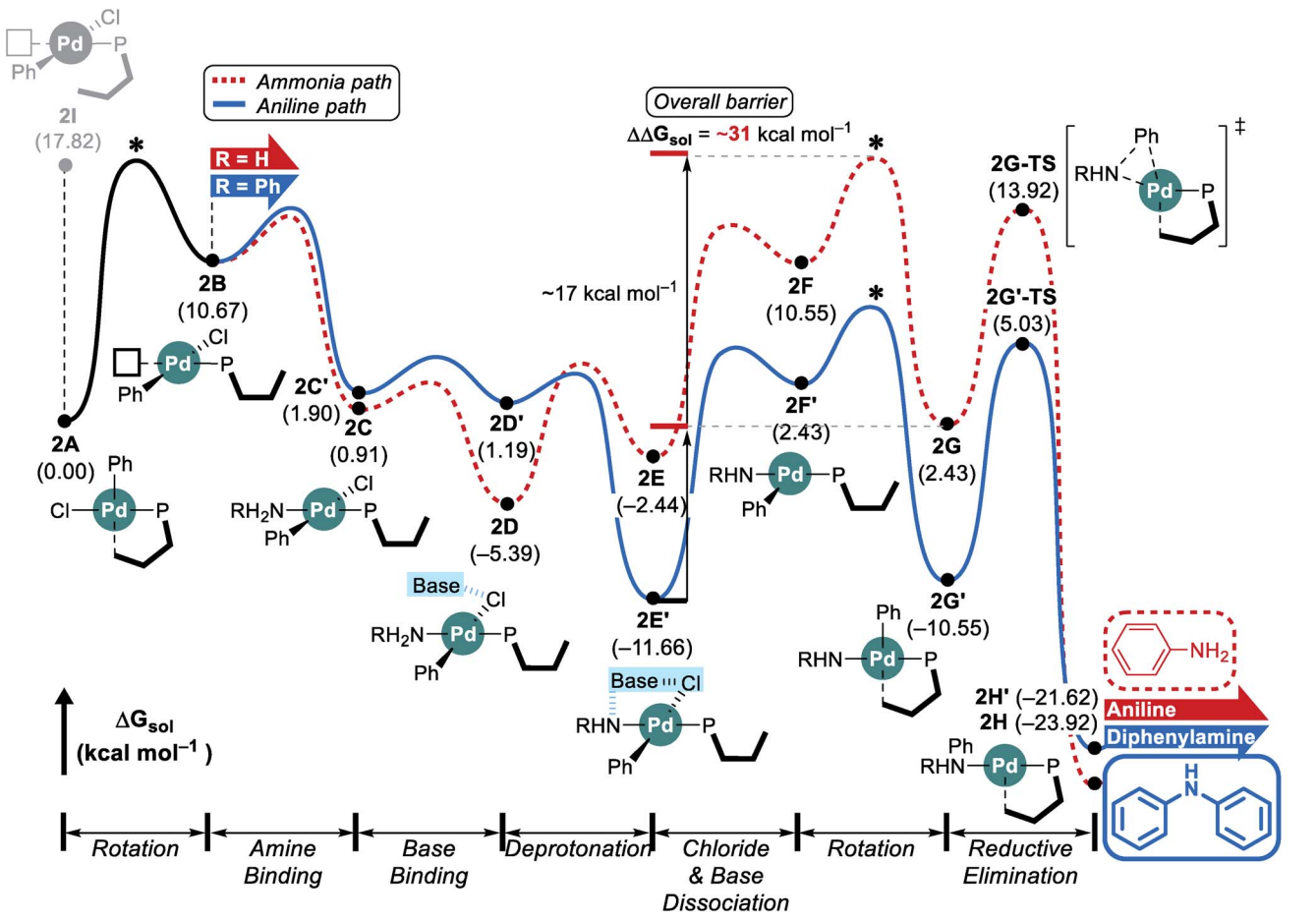

Fig. 3 DFT-calculated energy profile for Pd-catalyzed *N*-arylation with **L2**. * represents the estimated rotation barrier which is estimated to be over 17 kcal mol^{-1}.

if the reaction were to be allowed to reach full conversion. Note that the reaction with **L1** which gives diphenylamine dominantly ran for 16 h while the reaction with **L2** was run only for 5 h (Scheme 1).

Mechanism using L3

Fig. 4 shows the reaction energy profile of the catalytic reaction with the **L3** ligand. In this case, the bulkier alkyl group on the phosphorus further disturbs the rotation in intermediate **3A** and the proximal form of **L3** is maintained throughout the whole catalytic cycle, as illustrated in Fig. 4. While the distal pathway is also examined as an alternative pathway considering the small energy difference between the proximal intermediate **3B** and the estimated rotation barrier, this possibility is discarded since it cannot explain the observed selectivity (see ESI† for details).

Once the rearranged intermediate **3B** is formed, our proposed mechanism proceeds with the amine binding and subsequent deprotonation without releasing the sterically induced stress based on the proximal orientation of the phosphine ligand. Consequently, the early phase of the catalytic cycle shows much higher, but still accessible intermediate energies. The ammonia adduct **3C** is located at 15.5 kcal mol^{-1} and the subsequent binding of the NaO^{t}Bu tetramer affords intermediate **3D** at 7.6 kcal mol^{-1}. Deprotonation and chloride extraction ultimately result in the formation of the intermediate **3G** at −4.3 kcal mol^{-1}, which can easily undergo reductive elimination *via* the transition state **3H-TS** to produce aniline. Because of the steric crowding associated with the proximal form of the phosphine ligand, this reductive elimination barrier is relatively low and our calculations suggest that the ammonia binding step (**3B** → **3C**) is most difficult in this reaction. As discussed above, we again considered adding an aniline substrate to intermediate **3B** instead of ammonia, shown in blue in Fig. 4. With the phosphine ligand locked in the proximal arrangement, the amine adduct **3C′** is found at 18.1 kcal mol^{-1}. The proton shift transition state **3D′-TS** requires 20.1 kcal mol^{-1}. Once the intermediate **3H′** is reached, the reductive elimination to form the final product is relatively easy with the transition state **3H′-TS** being at 9.4 kcal mol^{-1}. Comparing this reaction energy profile to that discussed for the **L1** ligand, significant differences can be identified. The inability to release the steric repulsion encountered in the proximal configuration of the phosphine ligand forces the early phase of the reaction to be higher in energy so that the amine binding step or *tert*-butanol dissociation step which is part of the deprotonation process could influence the product selectivity. With the amine binding being the rate determining step, this catalytic cycle will provide aniline dominantly because the

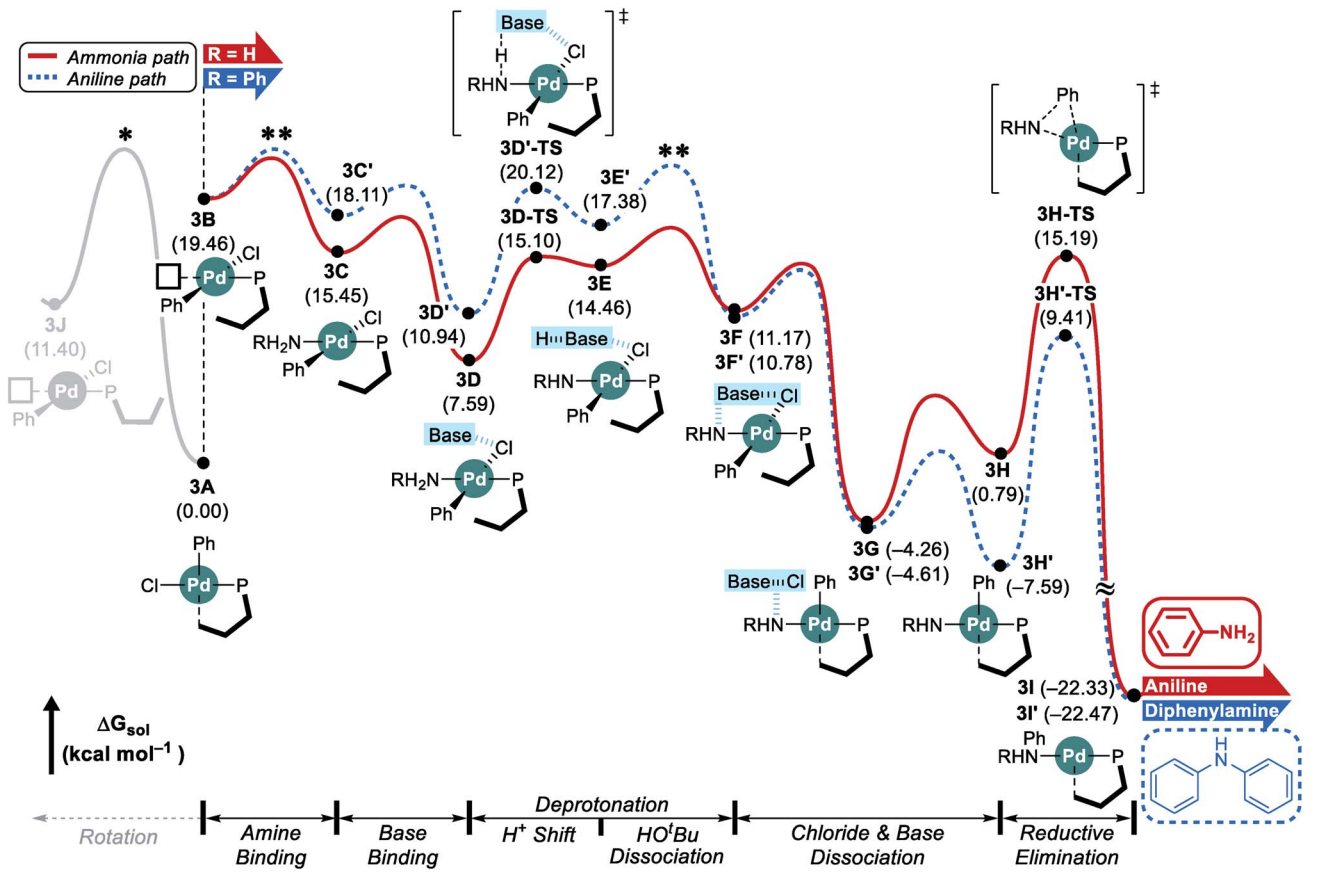

Fig. 4 DFT-calculated energy profile for Pd-catalyzed *N*-arylation with **L3**. * represents the estimated rotation barrier which is estimated to be over 21 kcal mol^{-1}. ** represents predicted selectivity determining states.

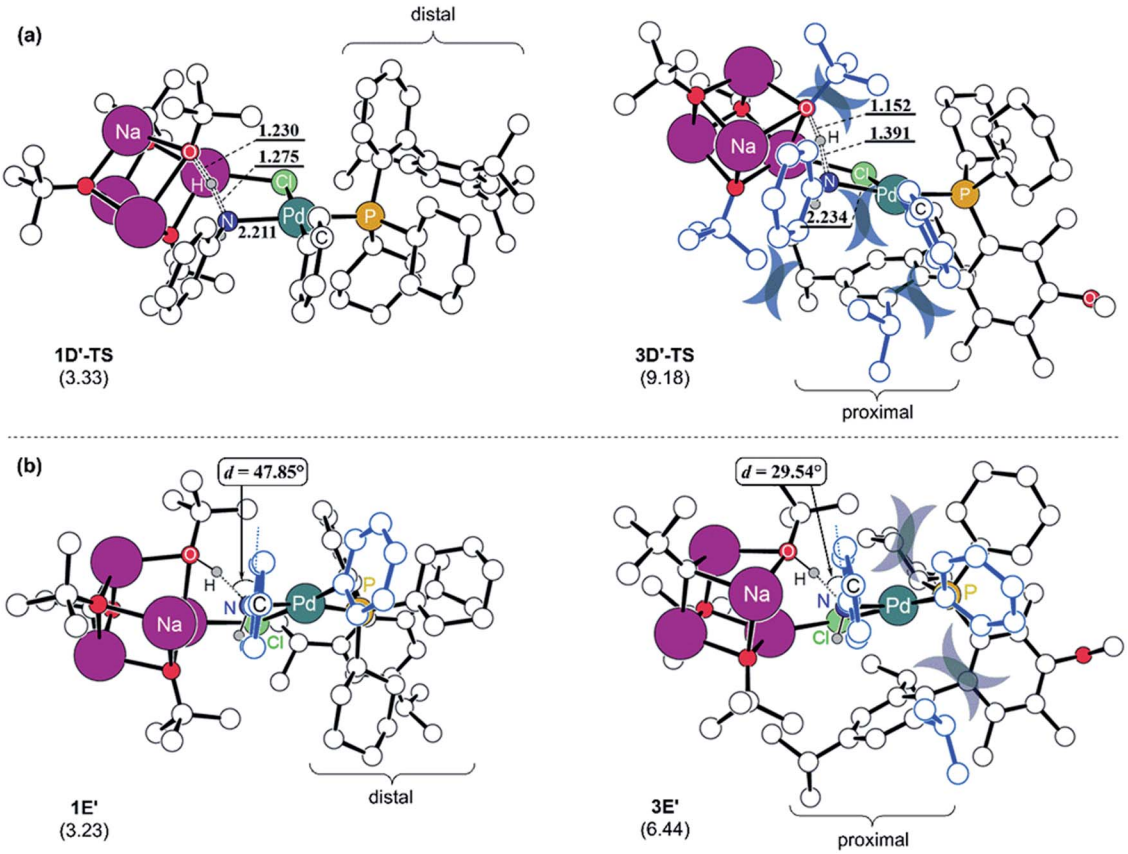

Fig. 5 Optimized structures of (a) aniline-deprotonation transition states and (b) proton-shifted intermediates with **L1** and **L3**. Relative free energies in kcal mol^{-1} referenced to **1D′** and **3D′**, respectively, are given in parentheses and key distances are given in Å. The molecular components responsible for steric repulsion are coloured in dark blue.

stronger nucleophilicity of ammonia in addition to the higher concentration of 3 equivalents promotes the generation of **3C** over **3C′**. Alternatively, the deprotonation could determine the selectivity: unlike in the case of **L1**, the ammonia substrate is preferred by nearly 5 kcal mol^{-1} at the proton shift transition states **3D-TS** and **3D′-TS**. In addition, the intermediate **3E′** is 2.9 kcal mol^{-1} higher in energy than **3E**, leading to a higher probability of *tert*-butanol dissociation **3E′**. While the dissociation barrier could not be explicitly located in the DFT method and thus, we could not compare the dissociation preference quantitatively, it is reasonable to assume that the barrier from **3E′** would be higher by following Hammond's postulate. In conclusion, these reaction energy profiles suggest that as long as ammonia is present, the Pd-catalyst will prefer ammonia over aniline as the reaction substrate.

To understand the reason for the arduous aniline deprotonation process in the **L3** system, the four structures involved in the proton-shift, **1D′-TS** and **1E′** in the **L1** system, and **3D′-TS** and **3E′** in the **L3** system are analysed in greater detail and illustrated in Fig. 5. The shorter O–H and longer N–H distances of **3D′-TS** represent a late transition state, whereas the Pd–N bond which is also expected to be shorter according to the reaction progress is 0.023 Å longer and contributes to the higher barrier. The late transition state with respect to the deprotonation trajectory and the elongated Pd–N bond stem from the increased steric clash of the proximal-form. The late transition state is enforced by the bulkiness of the ^{i}Pr substituent which is incorporated at the *para*-position of biaryl. This steric bulk determines the aniline-Ph orientation and enhances the repulsive interaction between the Ph and the *tert*-butoxide moiety in the early phase of the trajectory. Therefore, the saddle point is necessarily pushed to a late phase of the transition where the intense repulsive interaction is resolved to a higher degree. Furthermore, the elongation of the Pd–N bond is governed by the steric bulk of *ortho*-^{i}Pr which distorts the Ph on the Pd towards the Ph of the aniline and increases the repulsive steric interaction between them. As a result, the aniline proton shift barrier becomes 5.9 kcal mol^{-1} higher in the **L3** system. The increased steric clash of the proximal form, especially the distorted Ph on the Pd, makes the intermediate resulting from the proton shift unstable. As shown in Fig. 5b, the proton shift of aniline is 6.4 kcal mol^{-1} uphill in **L3** while that in **L1** is only 3.2 kcal mol^{-1} uphill in energy. The optimized structures of the intermediates **1E′** and **3E′** clearly depict the reason for these energies. As discussed above, the favorable deprotonation property of aniline over ammonia is a result of the π-resonance. In the case of **3E′**, this resonance is less likely to be maintained because the dihedral angle between the lone pair of the

nitrogen and the Ph-plane of aniline is forced to be only 29.5° due to steric interactions from the Ph moiety on the Pd while **1E′** shows a dihedral angle of 47.8° without that steric demand.

The mechanism using **L4** is nearly identical to that of **L3** and is not described in detail here, but establishes that the features we describe are generally applicable to different ligand systems.

Conclusions

In conclusion, we studied the mechanism of the Pd-catalyzed *N*-arylation of ammonia and identified the reasons for the chemoselectivity observed as the nature of the phosphine ligand is varied by functionalization. The chemoselectivity is determined by a synergistic steric effect from the bulkiness of NaO^{t}Bu base, which is proposed to exist in a tetrameric form under the given conditions, and the steric demands of the ligands, where the rotation of the biaryl moiety of the phosphine ligand is severely hindered to force the phosphine ligand to maintain a proximal arrangement throughout the entire reaction. If sterically less encumbered ligands are used, the phosphine ligand can easily rotate the biaryl moiety to adopt the distal form, which releases much of the steric crowding that results from the addition of the amine substrate. The chemoselectivity observed for the proposed distal mechanism is ultimately the result of the pK_a difference between ammonia and aniline that is expressed in a much easier deprotonation step, resulting in the preferential formation of the diphenylamine product. In the case of the proximal mechanism, the increased steric crowding pushes the early phase of the reaction trajectory towards higher energy and switches the selectivity determining state to the amine binding or the deprotonation process. Ammonia not only has a stronger binding affinity to Pd but also displays an easier proton shift ability due to the reduced steric crowding, which plays a key role in determining the chemoselectivity. Overall, this study offers a precise view on the two distinct reaction channels enabled by the dialkyl biaryl phosphine ligated catalyst and highlights how the bulkiness and rigidity of the ligand determine which channel becomes mechanistically relevant.

Conflicts of interest

There are no conflicts to declare.

Acknowledgements

MHB acknowledges financial support from the Institute for Basic Science (IBS-R10-A1). We thank Prof. Stephen L. Buchwald and his group for fruitful discussions.

Notes and references

1 P. Ruiz-Castillo and S. L. Buchwald, *Chem. Rev.*, 2016, **116**, 12564–12649.
2 S. Enthaler, *ChemSusChem*, 2010, **3**, 1024–1029.
3 P. T. Anastas and M. M. Kirchhoff, *Acc. Chem. Res.*, 2002, **35**, 686–694.
4 M. Appl, *Ammonia: Principles and Industrial Practice*, Wiley-VCH, Weinheim, 1999.
5 J. I. van der Vlugt, *Chem. Soc. Rev.*, 2010, **39**, 2302–2322.
6 D. M. Roundhill, *Chem. Rev.*, 1992, **92**, 1–27.
7 J. L. Klinkenberg and J. F. Hartwig, *Angew. Chem., Int. Ed.*, 2011, **50**, 86–95.
8 J. Zhao, A. S. Goldman and J. F. Hartwig, *Science*, 2005, **307**, 1080–1082.
9 C. Lombardi, J. Day, N. Chandrasoma, D. Mitchell, M. J. Rodriguez, J. L. Farmer and M. G. Organ, *Organometallics*, 2017, **36**, 251–254.
10 M. Fan, W. Zhou, Y. Jiang and D. Ma, *Org. Lett.*, 2015, **17**, 5934–5937.
11 R. A. Green and J. F. Hartwig, *Angew. Chem., Int. Ed.*, 2015, **127**, 3839–3843.
12 P. G. Alsabeh, R. J. Lundgren, R. McDonald, C. C. C. Johansson Seechurn, T. J. Colacot and M. Stradiotto, *Chem.–Eur. J.*, 2013, **19**, 2131–2141.
13 R. J. Lundgren, B. D. Peters, P. G. Alsabeh and M. Stradiotto, *Angew. Chem., Int. Ed.*, 2010, **49**, 4071–4074.
14 G. D. Vo and J. F. Hartwig, *J. Am. Chem. Soc.*, 2009, **131**, 11049–11061.
15 C. W. Cheung, D. S. Surry and S. L. Buchwald, *Org. Lett.*, 2013, **15**, 3734–3737.
16 D. S. Surry and S. L. Buchwald, *J. Am. Chem. Soc.*, 2007, **129**, 10354–10355.
17 A. D. Bochevarov, E. Harder, T. F. Hughes, J. R. Greenwood, D. A. Braden, D. M. Philipp, D. Rinaldo, M. D. Halls, J. Zhang and R. A. Friesner, *Int. J. Quantum Chem.*, 2013, **113**, 2110–2142.
18 A. D. Becke, *Phys. Rev. A: At., Mol., Opt. Phys.*, 1988, **38**, 3098–3100.
19 C. Lee, W. Yang and R. G. Parr, *Phys. Rev. B: Condens. Matter Mater. Phys.*, 1988, **37**, 785–789.
20 S. Grimme, J. Antony, S. Ehrlich and H. Krieg, *J. Chem. Phys.*, 2010, **132**, 154104.
21 R. Ditchfield, W. J. Hehre and J. A. Pople, *J. Chem. Phys.*, 1971, **54**, 724–728.
22 W. J. Hehre and W. A. Lathan, *J. Chem. Phys.*, 1972, **56**, 5255–5257.
23 V. A. Rassolov, M. A. Ratner, J. A. Pople, P. C. Redfern and L. A. Curtiss, *J. Comput. Chem.*, 2001, **22**, 976–984.
24 P. J. Hay, P. Jeffrey Hay and W. R. Wadt, *J. Chem. Phys.*, 1985, **82**, 270–283.
25 W. R. Wadt and P. Jeffrey Hay, *J. Chem. Phys.*, 1985, **82**, 284–298.
26 P. J. Hay, P. Jeffrey Hay and W. R. Wadt, *J. Chem. Phys.*, 1985, **82**, 299–310.
27 T. H. Dunning, *J. Chem. Phys.*, 1989, **90**, 1007–1023.
28 D. J. Tannor, B. Marten, R. Murphy, R. A. Friesner, D. Sitkoff, A. Nicholls, B. Honig, M. Ringnalda and W. A. Goddard III, *J. Am. Chem. Soc.*, 1994, **116**, 11875–11882.
29 B. Marten, K. Kim, C. Cortis, R. A. Friesner, R. B. Murphy, M. N. Ringnalda, D. Sitkoff and B. Honig, *J. Phys. Chem.*, 1996, **100**, 11775–11788.
30 W. J. Hehre, R. Ditchfield, R. F. Stewart and J. A. Pople, *J. Chem. Phys.*, 1970, **52**, 2769–2773.

31 C. L. McMullin, B. Rühle, M. Besora, A. G. Orpen, J. N. Harvey and N. Fey, *J. Mol. Catal. A: Chem.*, 2010, **324**, 48–55.
32 B. H. Yang and S. L. Buchwald, *J. Organomet. Chem.*, 1999, **576**, 125–146.
33 T. E. Barder and S. L. Buchwald, *J. Am. Chem. Soc.*, 2007, **129**, 12003–12010.
34 J. F. Hartwig, S. Richards, D. Barañano and F. Paul, *J. Am. Chem. Soc.*, 1996, **118**, 3626–3633.
35 S. Shekhar and J. F. Hartwig, *Organometallics*, 2007, **26**, 340–351.
36 T. R. Cundari and J. Deng, *J. Phys. Org. Chem.*, 2005, **18**, 417–425.
37 F. Barrios-Landeros and J. F. Hartwig, *J. Am. Chem. Soc.*, 2005, **127**, 6944–6945.
38 F. Barrios-Landeros, B. P. Carrow and J. F. Hartwig, *J. Am. Chem. Soc.*, 2009, **131**, 8141–8154.
39 S. Shekhar, P. Ryberg, J. F. Hartwig, J. S. Mathew, D. G. Blackmond, E. R. Strieter and S. L. Buchwald, *J. Am. Chem. Soc.*, 2006, **128**, 3584–3591.
40 J. F. Hartwig, *Inorg. Chem.*, 2007, **46**, 1936–1947.
41 M. Ahlquist and P.-O. Norrby, *Organometallics*, 2007, **26**, 550–553.
42 Y. Sunesson, E. Limé, S. O. Nilsson Lill, R. E. Meadows and P.-O. Norrby, *J. Org. Chem.*, 2014, **79**, 11961–11969.
43 T. Ikawa, T. E. Barder, M. R. Biscoe and S. L. Buchwald, *J. Am. Chem. Soc.*, 2007, **129**, 13001–13007.
44 J. F. Hartwig, *Acc. Chem. Res.*, 1998, **31**, 852–860.
45 J. P. Wolfe, S. Wagaw, J.-F. Marcoux and S. L. Buchwald, *Acc. Chem. Res.*, 1998, **31**, 805–818.
46 J. Hartwig, *Synlett*, 1997, **1997**, 329–340.
47 D. S. Surry and S. L. Buchwald, *Chem. Sci.*, 2011, **2**, 27–50.
48 M. R. Biscoe, T. E. Barder and S. L. Buchwald, *Angew. Chem., Int. Ed.*, 2007, **119**, 7370–7373.
49 L. M. Jackman and B. C. Lange, *J. Am. Chem. Soc.*, 1981, **103**, 4494–4499.
50 D. Seebach, *Angew. Chem., Int. Ed.*, 1988, **27**, 1624–1654.
51 W.-B. Liu, D. P. Schuman, Y.-F. Yang, A. A. Toutov, Y. Liang, H. F. T. Klare, N. Nesnas, M. Oestreich, D. G. Blackmond, S. C. Virgil, S. Banerjee, R. N. Zare, R. H. Grubbs, K. N. Houk and B. M. Stoltz, *J. Am. Chem. Soc.*, 2017, **139**, 6867–6879.